Isotropization of Quaternion-Neural-Network-Based PolSAR Adaptive Land Classification in Poincare-Sphere Parameter Space

doi: 10.1109/LGRS.2018.2831215

Isotropization of Quaternion-Neural-Network-Based PolSAR Adaptive Land Classification in Poincare-Sphere Parameter Space

Kazutaka Kinugawa, Fang Shang, *Member, IEEE,* Naoto Usami, and Akira Hirose, *Fellow, IEEE*

***Abstract*—Quaternion neural networks (QNNs) achieve high accuracy in polarimetric synthetic aperture radar (PolSAR) classification for various observation data by working in Poincare-sphere-parameter space. The high performance arises from the good generalization characteristics realized by a QNN as three-dimensional rotation as well as amplification/attenuation, which is in good consistency with the isotropy in the polarization-state representation it deals with. However, there are still two anisotropic factors so far which lead to a classification capability degraded from its ideal performance. In this paper, we propose an isotropic variation vector and an isotropic activation function to improve the classification ability. Experiments demonstrate the enhancement of the QNN ability.**

I. Introduction

Space-borne and airborne polarimetric synthetic aperture radar (PolSAR) is useful in collecting global and precise land-use information. For land classification use, many supervised and unsupervised analysis methods have been reported [1]–[3]. Previously, we proposed Stokes-vector-based classification algorithms [4], [5]. By focusing on a local window, we introduced two parameters to describe the features of local averaged Stokes vectors, i.e., the position vector, and its variation vector. Since the Stokes vector can be expressed by a point on/in Poincare sphere, we named them together Poincare sphere parameters. One of the merits of using Poincare sphere parameters lies in the model-free use of degree of polarization information, which is a parameter meaningful to represent scattering features [6]–[8].

There in [4], we employ quaternion neural network (QNN) to realize robust supervised learning in adaptive classification in the Poincare-sphere-parameter space. Unlike a conventional real valued neural network, all of the parameters in QNN are quaternions. It has high capability in dealing with rotation and scaling of three-dimensional (3-D) vectors [9], [10] in consistency with the Poincare sphere isotropy [4], showing a high generalization ability. However, there are two anisotropic factors in the previously proposed neural dynamics which lead to a classification capability degraded from its ideal performance. The two anisotropic factors lie in the variation vector of Poincare-sphere parameters, and the activation function of the QNN. First, no matter how the position vectors distribute on/in the Poincare sphere, components of the conventional variation vector are always positive values, lacking consistency with the rotational / scaling transform property of QNNs. Besides, when the polarization is more uniform, the variation vector has a smaller norm. Though this nature agrees with the name of "variance", such a small norm influences the neurodynamics only a little. This is inconsistent with the fact that a uniform polarization has stronger meaning in most land classification tasks. Second, with the conventional activation function, the position vectors are processed unevenly dependently on their position (direction) on/in the Poincare sphere. This is also against the isotropy of QNN and the Poincare sphere space.

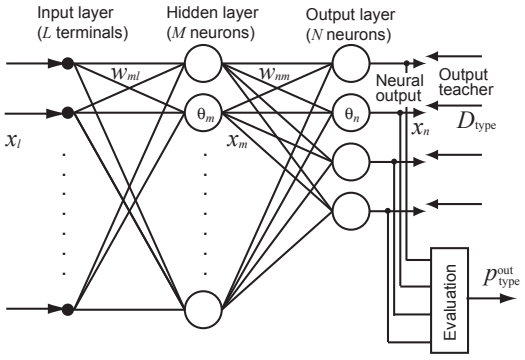

Fig. 1. Structure of the quaternion neural network employed in the experiments.

In this paper, by considering the two factors above, we propose an isotropic variation vector and an isotropic activation function. We show the results of classification experiments for ALOS-2 PALSAR2 data of Tomakomai area, Japan. The results show a great improvement in the classification ability of the QNN with the proposals in comparison with the conventional method.

II. Previously Proposed Neuraldynamics

We first describe the previously proposed quaternion neural-network-based adaptive land classification in Poincare-sphere-parameter space [4], [11], [12].

A part of this work was supported by JSPS KAKENHI Grant Number 15H02756 and 18H04105, and also by KDDI Foundation.

K. Kinugawa, N. Usami and A. Hirose are with the Department of Electrical Engineering and Information Systems, The University of Tokyo, Tokyo 113-8656, Japan.

F. Shang was with the Department of Electrical Engineering and Information Systems, The University of Tokyo, Tokyo 113-8656, Japan, and is currently with the Department of Computer and Network Engineering, University of Electro-Communications, 1-5-1 Chofugaoka, Chofu, Tokyo 182-8585, Japan.

A. Poincare Sphere Parameters for Characterizing Targets

A PolSAR system in fully polarimetric mode obtains a scattering matrix $\boldsymbol{S}$ for each pixel in an observation area expressed as

$$\boldsymbol{S} = \begin{bmatrix} S_{\mathrm{HH}} & S_{\mathrm{HV}} \\ S_{\mathrm{VH}} & S_{\mathrm{VV}} \end{bmatrix} \tag{1}$$

where H and V represent horizontal and vertical polarizations, respectively. The incident wave $\boldsymbol{E}^{\mathrm{i}} = [E^{\mathrm{i}}_{\mathrm{H}} \ E^{\mathrm{i}}_{\mathrm{V}}]^T$ and the corresponding scattered and received wave $\boldsymbol{E}^{\mathrm{r}} = [E^{\mathrm{r}}_{\mathrm{H}} \ E^{\mathrm{r}}_{\mathrm{V}}]^T$ are related by $\boldsymbol{S}$ as

$$\begin{bmatrix} E^{\mathrm{r}}_{\mathrm{H}} \\ E^{\mathrm{r}}_{\mathrm{V}} \end{bmatrix} = \begin{bmatrix} S_{\mathrm{HH}} & S_{\mathrm{HV}} \\ S_{\mathrm{VH}} & S_{\mathrm{VV}} \end{bmatrix} \begin{bmatrix} E^{\mathrm{i}}_{\mathrm{H}} \\ E^{\mathrm{i}}_{\mathrm{V}} \end{bmatrix} \tag{2}$$

From the scattered and received wave $\boldsymbol{E}^{\mathrm{r}} = [E^{\mathrm{r}}_{\mathrm{H}} \ E^{\mathrm{r}}_{\mathrm{V}}]^T$, the averaged Stokes vector is calculated as

$$\begin{bmatrix} g_0 \\ g_1 \\ g_2 \\ g_3 \end{bmatrix} = \begin{bmatrix} \langle E^{\mathrm{r}}_{\mathrm{H}} {E^{\mathrm{r}}_{\mathrm{H}}}^* \rangle + \langle E^{\mathrm{r}}_{\mathrm{V}} {E^{\mathrm{r}}_{\mathrm{V}}}^* \rangle \\ \langle E^{\mathrm{r}}_{\mathrm{H}} {E^{\mathrm{r}}_{\mathrm{H}}}^* \rangle - \langle E^{\mathrm{r}}_{\mathrm{V}} {E^{\mathrm{r}}_{\mathrm{V}}}^* \rangle \\ \langle E^{\mathrm{r}}_{\mathrm{H}} {E^{\mathrm{r}}_{\mathrm{V}}}^* \rangle + \langle E^{\mathrm{r}}_{\mathrm{V}} {E^{\mathrm{r}}_{\mathrm{H}}}^* \rangle \\ j(\langle E^{\mathrm{r}}_{\mathrm{H}} {E^{\mathrm{r}}_{\mathrm{V}}}^* \rangle - \langle E^{\mathrm{r}}_{\mathrm{V}} {E^{\mathrm{r}}_{\mathrm{H}}}^* \rangle) \end{bmatrix} \tag{3}$$

where $\langle \cdot \rangle$ means ensemble averaging process in $L_{\mathrm{pos}} \times L_{\mathrm{pos}}$ pixel area and $(\cdot)^*$ denotes the complex conjugate.

With quaternion concept, we define the position vector $\boldsymbol{P}$ as

$$\boldsymbol{P} \equiv \left[P^{(e)} \ P^{(i)} \ P^{(j)} \ P^{(k)} \right]^T \equiv \left[0 \ \frac{g_1}{g_0} \ \frac{g_2}{g_0} \ \frac{g_3}{g_0} \right]^T \tag{4}$$

which is corresponding to a point on/in a unit sphere called Poincare sphere. The position vector describes the position of its corresponding point on/in the Poincare sphere. The variation vector $\boldsymbol{\sigma}$ is defined as

$$\begin{aligned} \boldsymbol{\sigma} &\equiv \left[\sigma^{(e)} \ \sigma^{(i)} \ \sigma^{(j)} \ \sigma^{(k)} \right]^T \\ \sigma^{(\nu)} &\equiv \sqrt{\frac{1}{N_\sigma - 1} \sum_{\xi=1}^{N_\sigma} \{ P^{(\nu)}_{\xi} - \overline{P^{(\nu)}} \}^2} \end{aligned} \tag{5}$$

where $N_\sigma \equiv L_\sigma \times L_\sigma$ expresses the number of pixels of a local window at calculating the standard deviations, the subscript ξ is the index for the pixels in the window, ν should be e, i, j or k, and $\overline{P^{(\nu)}}$ is the mean of $P^{(\nu)}$ in the window. The variation vector represents the spatial fluctuation of the position vector. Since both of the proposed vectors have close relationship with the Poincare sphere, we named the set of the position and variation vectors the Poincare-sphere parameters. The Poincare-sphere parameters for each sample pixel are used for training process of the quaternion neural network.

B. Quaternion Neural Networks for Adaptive Classification

In our previous work [4], land classification is conducted by a quaternion neural network (QNN) processing the Poincare-sphere parameters defined above. The structure of the QNN is shown in Fig. 1. Here, L, M, and N denote the numbers of the input terminals, hidden-layer neurons and output-layer neurons, respectively, and the subscripts l, m, and n are the index for the nodes in the input, hidden and output layers, respectively. Besides, $\boldsymbol{x}_l$ denotes the input quaternion of l-th neuron, $\boldsymbol{x}_m$ and $\boldsymbol{x}_n$ denote the output quaternion of m-th hidden and n-th output neurons, respectively, $\boldsymbol{w}_{ml}$ and $\boldsymbol{w}_{nm}$ denote the connection weights between l-th terminal and m-th neuron and that between m-th neuron and n-th neuron respectively, $\boldsymbol{\theta}_m$ and $\boldsymbol{\theta}_n$ denote the threshold of m-th and n-th neuron, respectively, D_{type} denotes the output teacher, and $p^{out}_{type} \in (0,\ 1)$ denotes the final output. If a pixel belongs to a certain "type" class, the corresponding p^{out}_{type} will be near to 1, otherwise, if the pixel is very different from the "type" class, p^{out}_{type} will be near to 0. The forward processing at the m-th neuron is expressed as

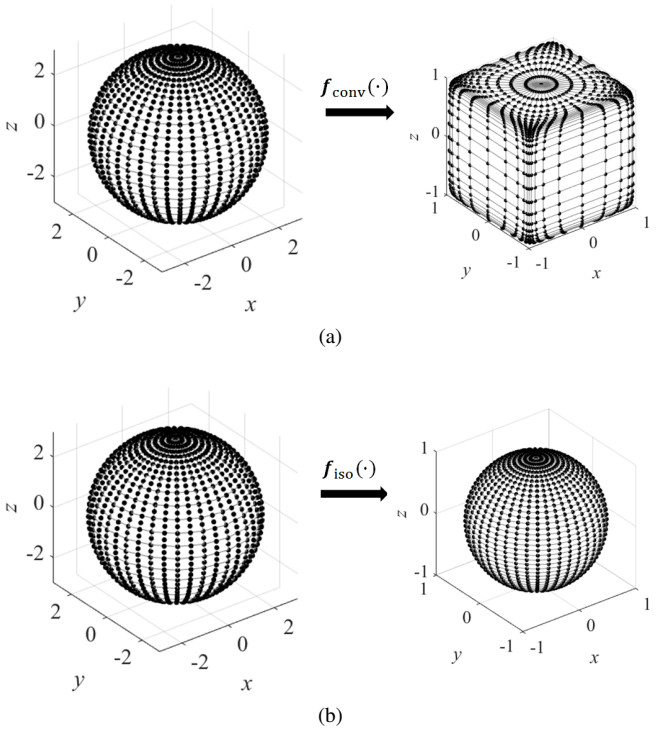

Fig. 2. Distributive features of originally isotropic data after mapping by (a) conventional anisotropic function $\boldsymbol{f}_{\mathrm{conv}}(\cdot)$, and (b) proposed isotropic function $\boldsymbol{f}_{\mathrm{iso}}(\cdot)$.

$$\boldsymbol{s}_m = \sum_i \frac{\boldsymbol{w}_{ml} \otimes \boldsymbol{x}_l \otimes \boldsymbol{w}^*_{ml}}{|\boldsymbol{w}_{ml}|} - \boldsymbol{\theta}_m \tag{6}$$

$$\boldsymbol{x}_m = \boldsymbol{f}(\boldsymbol{s}_m) \tag{7}$$

where $\boldsymbol{s}_m$ is the inner state of the neuron, $\otimes$ is the outer product process for quaternions, and $\boldsymbol{w}_{ml} \otimes \boldsymbol{x}_l \otimes \boldsymbol{w}^*_{ml}$ represents the rotation of $\boldsymbol{x}_l$ in 3-D space where the axis and angle of the rotation are defined by the neural weight $\boldsymbol{w}_{ml}$. The activation function $\boldsymbol{f}$ is defined in the previous paper [4] as

$$\begin{aligned} \boldsymbol{f}(\boldsymbol{s}) &\equiv \left[0 \ f(s^{(i)}) \ f(s^{(j)}) \ f(s^{(k)}) \right]^T \\ &= \left[0 \ \tanh s^{(i)} \ \tanh s^{(j)} \ \tanh s^{(k)} \right]^T \end{aligned} \tag{8}$$

where $\boldsymbol{s} \equiv [0 \ s^{(i)} \ s^{(j)} \ s^{(k)} \ ]^T$ is the quaternion representation by elements. The training process and the classification process are described in [4].

III. Isotropization of Quaternion Neural-Network-Based Adaptive Land Classification in Poincare-Sphere-Parameter Space

we make two proposals to realize isotropization for improving the generalization ability of QNNs.

A. Isotropization of Variation Vector

We express the conventional variation vector as $\boldsymbol{\sigma}_{\mathrm{conv}}$. The variation vector is summed up in a 3-D output space of each neuron. Moreover, it is only distributed in the $1/8$ space $\{(i,j,k)|i \geq 0, j \geq 0, k \geq 0\}$. It means that no matter how the position vectors distribute on/in the Poincare sphere, components of the conventional variation vector $\boldsymbol{\sigma}_{\mathrm{conv}}$ are always positive. Such a feature lacks consistency with the isotropy of the Poincare-sphere space. In addition, with the variation vector in (5), when the polarization is more uniform, the variation vector has a smaller norm influencing the neurodynamics only a little. This is inconsistent with the fact that a uniform polarization has stronger meaning in most land classification tasks.

The newly proposed isotropic variation vector is expressed as

---

Equation (10) on the next page

---

where $\overline{\boldsymbol{P}} \equiv [0 \ \ \overline{P^{(i)}} \ \overline{P^{(j)}} \ \overline{P^{(k)}}]^T$ is the average of position vectors in the local window. The parameter σ_r provides $\overline{\boldsymbol{P}}$ with the nonlinear scale based on the degree of the invariability in the 3-D space. In other words, the new variation vector contains two physical meanings, i.e., the average polarization state in a window as the direction as well as the spatial coherency as the norm.

B. Isotropization of Activation Function

From here, we note the conventional activation function as $\boldsymbol{f}_{\mathrm{conv}}$. Fig. 2a shows how this function maps input 3-D vectors, where vectors with length being 2 are taken as test samples. According to Fig. 2a, the input vectors distributed on a sphere are mapped to a cubic space with a side length of 2 and centered at the origin of the coordinate system. It means that, the effect of mapping process on a vector, i.e. the changes of length and direction, depends on the vector's spatial position. That is, the conventional activation function $\boldsymbol{f}_{\mathrm{conv}}$ is anisotropic. The position vector located in different positions present different polarization states. Since the physical meanings of these vectors have the same significance, the mathematical operations in a QNN should have fair effects on all different polarization states. Therefore, basically, the QNN algorithm, especially, the activation function in it, should be isotropic.

The newly proposed isotropic activation function is

$$\boldsymbol{f}_{iso}(\boldsymbol{s}) \equiv \frac{\tanh|\boldsymbol{s}|}{|\boldsymbol{s}|} \left[\ 0 \ s^{(i)} \ s^{(j)} \ s^{(k)} \ \right]^T \tag{9}$$

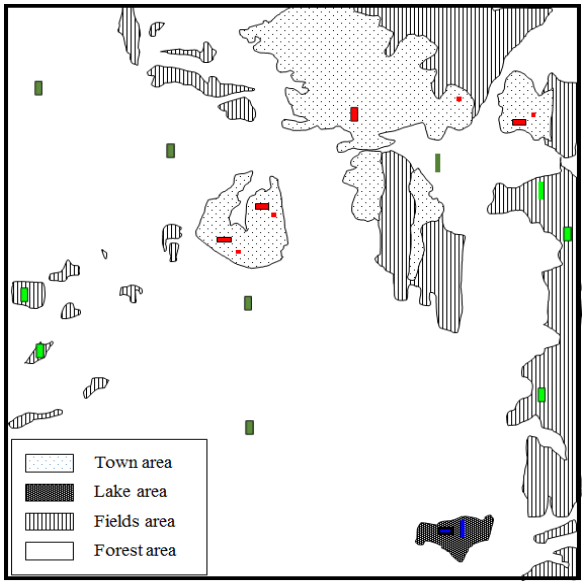

Fig. 3. Sketch of Tomakomai area. The small rectangles outlined by black boxes show sample areas for accuracy evaluation, and other rectangles show teaching signal areas (red: town area, blue: lake area, green: fields area, and dark green: forest area).

where $|\boldsymbol{s}| \equiv \sqrt{\{s^{(i)}\}^2 + \{s^{(j)}\}^2 + \{s^{(k)}\}^2}$. Fig. 2b shows how the proposed activation function maps input 3-D vectors. It shows that the proposed function compresses the norm of a vector independent of its direction. The proposed activation function is isotropic.

IV. Experiments and Results

The target area is Shinchitose Airport and its surrounding area in Tomakomai, Japan, observed by ALOS-2. The sketch of this area is shown in Fig. 3. The size of the data is 8000×3000 pixels. The experiment aims to classify the area into four classes, i.e., town, lake, fields, and forest. Note that we use "other" class to include the targets that cannot be assigned to these four classes. For each one of these four classes, a set of input-teacher signals including 1000 pixels in total is selected from the data. The selected input-teacher-signal areas are shown in Fig. 3 by color rectangles without black edges. The sample areas for evaluation are randomly selected from the total target image as shown by rectangles outlined with black edges, which include totally 8000 pixels in respective classes.

In order to compare the classification performance, four dynamics are implemented in the experiments, namely, QNNs with 1) $\boldsymbol{f}_{\mathrm{conv}}$ and $\boldsymbol{\sigma}_{\mathrm{conv}}$, 2) $\boldsymbol{f}_{\mathrm{iso}}$ and $\boldsymbol{\sigma}_{\mathrm{conv}}$, 3) $\boldsymbol{f}_{\mathrm{conv}}$ and $\boldsymbol{\sigma}_{\mathrm{iso}}$, and 4) $\boldsymbol{f}_{\mathrm{iso}}$ and $\boldsymbol{\sigma}_{\mathrm{iso}}$.

To calculate Poincare-sphere parameters, we suppose four incident waves, i.e., horizontal, vertical, 45 degree linearly polarized and left circular polarized waves with $L_{pos} = 5$ and $L_{\sigma} = 9$, respectively, resulting eight quaternions. Then the neuron number of the input layer L is 8. The neuron numbers of hidden layer M and output layer N are 8 and 4, respectively. In the training process, QNNs are trained with iterations of 100 times. The initial values of the connection weights and the threshold quaternions are chosen at random.

$$\boldsymbol{\sigma}_{\rm iso} \equiv \begin{bmatrix} 0 \\ \sigma^{(i)} \\ \sigma^{(j)} \\ \sigma^{(k)} \end{bmatrix} \equiv (1-\tanh\sigma_r)\overline{\boldsymbol{P}} \tag{10}$$

$$\sigma_r \equiv \sqrt{\frac{1}{N_\sigma - 1}\sum_{\xi=1}^{N_\sigma} |\boldsymbol{P}_\xi - \overline{\boldsymbol{P}}|^2} = \sqrt{\frac{1}{N_\sigma - 1}\sum_{\xi=1}^{N_\sigma} \left\{ (P_\xi^{(i)} - \overline{P^{(i)}})^2 + (P_\xi^{(j)} - \overline{P^{(j)}})^2 + (P_\xi^{(k)} - \overline{P^{(k)}})^2 \right\}}$$

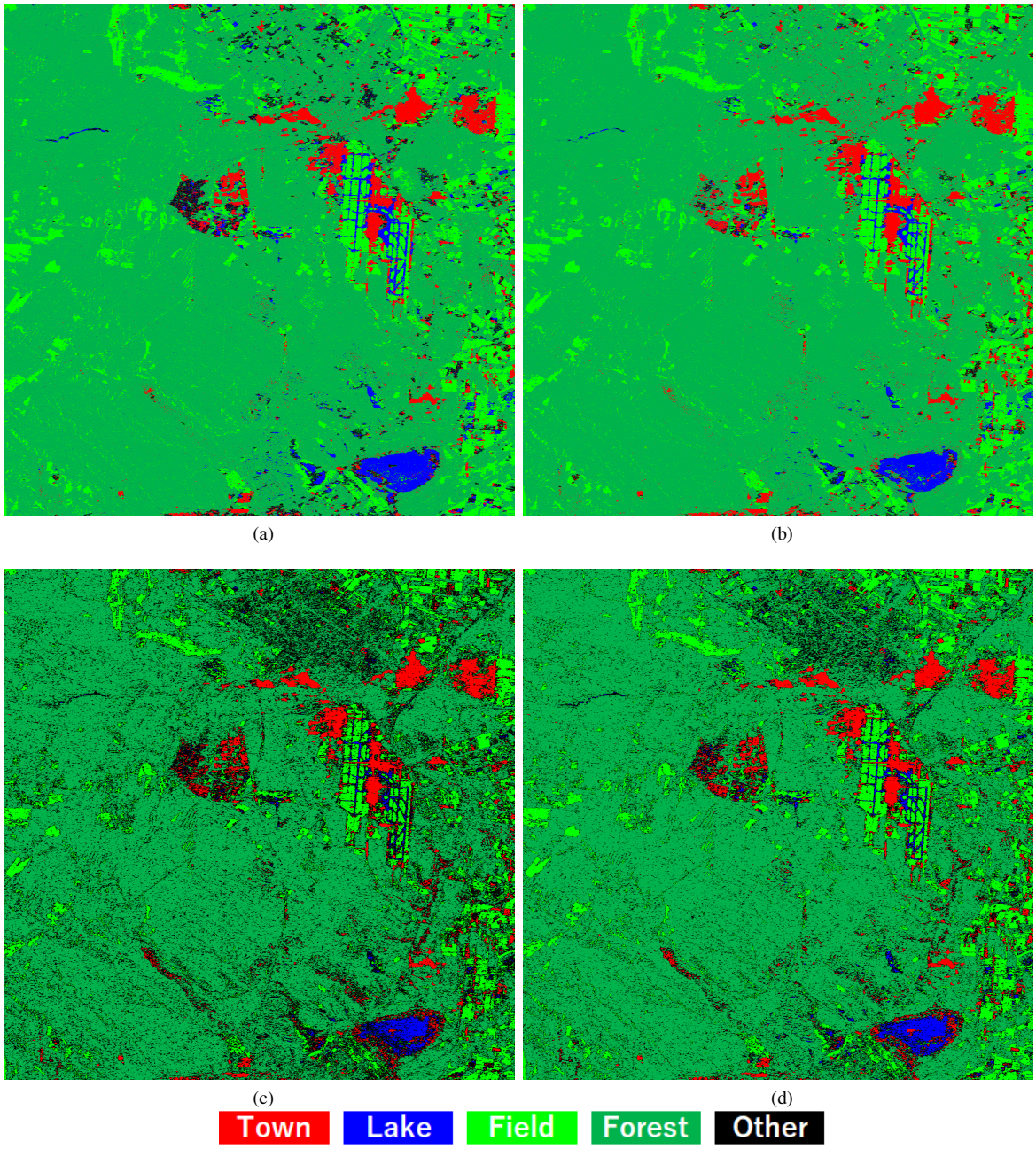

Fig. 4. Classification results for Tomakomai area having 8000 × 3000 pixels generated by QNN with a) $\boldsymbol{f}_{\rm conv}$ and $\boldsymbol{\sigma}_{\rm conv}$, b) $\boldsymbol{f}_{\rm iso}$ and $\boldsymbol{\sigma}_{\rm conv}$, c) $\boldsymbol{f}_{\rm conv}$ and $\boldsymbol{\sigma}_{\rm iso}$, and d) $\boldsymbol{f}_{\rm iso}$ and $\boldsymbol{\sigma}_{\rm iso}$.

The learning coefficient is 0.02. In the classification process, we assign a pixel to "type0" class, if ($P^{out}_{type0} > 0.9$) and ($P^{out}_{type} < 0.1 \quad \forall\ type \neq type0$), otherwise, we assign it to "other" class.

TABLE I
THE ACCURACY OF LAND-CLASSIFICATION RESULTS.

Method		Town	Lake	Fields	Forest	Others	Accuracy	Overall Accuracy
(a) Conv f Conv σ	Town	5722	111	12	543	1612	71.5%	79.5%
	Lake	4	6748	7	36	1205	84.4%	
	Fields	7	77	6083	697	1136	76.0%	
	Forest	15	4	307	6873	801	85.9%	
(b) Prop f Conv σ	Town	6070	225	9	417	1279	75.9%	81.3%
	Lake	0	6878	50	19	1053	86.0%	
	Fields	15	114	6393	436	1042	79.9%	
	Forest	4	8	541	6677	770	83.5%	
(c) Conv f Prop σ	Town	6004	5	2	143	1846	75.1%	77.7%
	Lake	0	6160	1	0	1839	77.0%	
	Fields	0	0	6500	215	1285	81.3%	
	Forest	0	0	209	6213	1578	77.7%	
(d) Prop f Prop σ	Town	6289	34	16	187	1474	78.6%	84.4%
	Lake	0	7188	0	6	806	89.9%	
	Fields	0	0	6974	388	638	87.2%	
	Forest	1	0	286	6545	1168	81.8%	

The experimental results are shown in Fig. 4. Focusing on two pairs of results, i.e., Fig. 4a and Fig. 4c, and, Fig. 4b and Fig. 4d, we can find that, with the conventional variation vector, most of the pixels of the big town area in the north of the test area are wrongly classified as forest class in Fig. 4a and Fig. 4b, whereas, with the proposed variation vector, most of these pixels are classified as "other" class. Since towns have various orientations, distributions, and/or dimensions, it is difficult to use limited teaching samples to cover all kinds of towns. Therefore, recognizing some towns as "other" is theoretically reasonable, and much better than wrong assignment. Moreover, if we focus on the other two result pairs, i.e., Fig. 4a and Fig. 4b, and, Fig. 4c and Fig. 4d, we can find that the results of the methods with the proposed activation function (Fig. 4b and Fig. 4d) have much fewer wrongly classified pixels in forest area than the results of methods without the proposed activation function (Fig. 4a and Fig. 4c). The comparisons above show that using the proposed variation vector and activation function, we can obtain higher classification performance.

Table I shows the classification accuracy of respective methods. The central four columns present the numbers of the pixels assigned to respective classes. The result shows quantitatively that the method with the proposed activation function and the proposed variation vector has the highest classification accuracy.

V. CONCLUSION

In this paper, we have proposed an isotropic variation vector and an isotropic activation function to improve the generalization ability in QNNs for PolSAR land classification. The experimental results have shown that the methods with the proposed variation vector have less wrongly classified pixels in the big town area in the north of the test area than the ones without the proposed variation vector. Moreover, the methods with the proposed activation function have lead to much fewer wrongly classified pixels in forest areas than the results of methods with the conventional activation function. With the proposals, higher classification performance have been achieved in quaternion-neural-network-based adaptive land classification in Poincare-sphere-parameter space.

REFERENCES

[1] J. S. Lee, W. M. Boerner, D. L. Schuler, T. L. Ainsworth, I. Hajnsek, K. P. Papathanassiou, and E. Luneburg, "A review of polarimetric SAR algorithms and their applications," *Journal of Photogrammetry and Remote Sensing*, vol. 9, pp. 31–80, 2004.

[2] S. R. Cloude and E. Pottier, "A review of target decomposition theorems in radar polarimetry," *IEEE Trans. Geosci. Remote Sens.*, vol. 34, pp. 498–518, 1996.

[3] R. Touzi, W. M. Boerner, J. S. Lee, and E. Lueneburg, "A review of polarimetry in the context of synthetic aperture radar: Concepts and information extraction," *Can. J. Remote Sensing*, vol. 30, pp. 380–407, 2004.

[4] F. Shang and A. Hirose, "Quaternion neural-network-based polsar land classification in poincare-sphere-parameter space," *IEEE Transactions on Geoscience and Remote Sensing*, vol. 52, pp. 5693 – 5703, 2014.

[5] ——, "Averaged stokes vector based polarimetric SAR data interpretation," *IEEE Transactions on Geoscience and Remote Sensing*, vol. 53, pp. 4536 – 4547, 2015.

[6] R. Touzi, S. Goze, T. L. Toan, A. Lopes, and E. Mougin, "Polarimetric discriminators for SAR images," *IEEE Trans. Geosci. Remote Sens.*, vol. 30, pp. 973–980, 1992.

[7] R. Shirvany, M. Chabert, and J. Y. Tourneret, "Ship and oil-spill detection using the degree of polarization in linear and hybrid/compact dual-PolSAR," *IEEE Journal of Selected Topics in Applied Earth Observations and Remote Sensing*, vol. 5, pp. 885–892, 2012.

[8] F. Shang and A. Hirose, "Considerations on C/T matrix-based PoLSAR land classification and explorations on stokes vector based method," in *IEEE International Geoscience and Remote Sensing Symposium*, 2014, pp. 4576–4579.

[9] A. Hirose, *Complex-valued Neural Networks (2nd edition)*. Springer, 2012.

[10] N. Matsui, T. Isokawa, H. Kusamichi, F. Peper, and H. Nishimura, "Quaternion neural network with geometrical operators," *Journal of Intelligent and Fuzzy Systems*, vol. 15, pp. 149–164, 2004.

[11] F. Shang and A. Hirose, "PolSAR land classification by using quaternion-valued neural networks," in *Asia-Pacific Conference on Synthetic Aperture Radar*, 2013, pp. 593–596.

[12] ——, "Use of poincare sphere parameters for fast supervised PolSAR land classification," in *IEEE International Geoscience and Remote Sensing Symposium*, 2013, pp. 3175–3178.